International Journal of Advanced Multidisciplinary Research and Studies

Consequence of flow and heat transfer analysis in a quadratic mixed convection magneto-micropolar nanofluid induced by an expanded stretching

[1] Akanbi OO, [2] Fatunmbi EO
[1, 2] Department of Mathematics and Statistics, Federal Polytechnic, Ilaro, Nigeria

Corresponding Author: **Akanbi OO**

Abstract

This specific study investigates the flow and heat transfer analysis in a quadratic mixed convection magneto-micropolar nanofluid over a vertically stretched sheet. The electro-conducting reactive micropolar fluid contains tiny nanoparticles in the presence of viscous dissipation, Joulean heating, Brownian movement of microscopic particles, thermal radiation, thermo-migration of particles, and prescribed surface temperature. Appropriate similarity variables are imposed on the mathematical equations to transform the partial derivatives governing the flow equations into ordinary derivatives, allowing for the numerical solution through the Runge-Kutta Fehlberg technique alongside shooting method. The parametric analysis of the physical quantities on the transport fields are illustrated by means of graphs while the findings show that an increase in the magnetic field term decelerates the velocity profiles of the micropolar fluid nanofluid while simultaneously reducing the thickness of the boundary layer of momentum. Furthermore, the concentration field of the nanoparticles profile decreases when the chemical reaction and Brownian motion parameters escalate whereas thermal radiation term raises the heat distribution across the surface.

1. Introduction

Researchers have paid a great deal of attention to the flow of fluids at the bounding surface and formed by expanding materials because of its significance in industrial and technical processes. Stretching sheet in a stationary cooling fluid is crucial in various manufacturing processes such as plastic sheets, glass manufacturing, hot rolling, wire drawing, manufacturing of paper and textiles (Ishak, 2008; Elbashbeshy *et al.*, 2018). The investigation of boundary layer flow occasioned by a stretching sheet was first examined by Crane (1970) [5]. The author reported a closed form solution for the flow profile. An extension to this concept was then extended by Gupta and Gupta (1977) [12] to a permeable surface. Many researchers have also extended this type of study on various configurations, conditions and parameters of interest (see Kumar, 2009 [14]; Makinde and Aziz, 2011 [18]; Akinbobola and Okoya, 2015 [2]; Fatunmbi and Fenuga, 2018).

Nanofluids are defined as liquids containing nanoparticles of materials like metals, oxides, carbides, etc. This novel family of fluids helps thermal conductivity and heat transmission as contrasted with the conventional heat transfer fluids like water, oil, ethylene glycol, etc. As described by Choi [1], nanofluid is a new class of heat transfer fluids that which consist a traditional fluid and nanoparticles. Recent research on nanofluid has shown that nanoparticles change the fluid characteristics because thermal conductivity of these particles is higher than convectional fluids. Heating and cooling are common phenomenon in a wide range of industrial and engineering processes, from the production of electricity to the operation of nuclear reactors, transportation industries, pharmaceutical and drug production, etc. Nanofluids have the ability to increase cooling process and raise heat transfer mechanism in high-energy equipment. The mix of the micropolar fluid with microscopic nanoparticles is crucial in varied domains of engineering, manufacturing, research and technology. Biomedical engineering, for example, involves the study of fluid dynamics in the brain and blood, as well as the drawing of metal filaments, the rheology of paints and other chemicals, the manufacture of medications, and other fields. On the foundation of these vital applications, numerous researchers have showed interest in such researches. For instance, Akba *et al.*, (2013) [1] evaluated the flow of hydromagnetic-nanofluid near a stagnation point alongside with radiation and conditioned by a convective surface heating while Noor *et al.*, (2015) [21] numerically reported such a study using micropolar nanofluid over a vertically stretched surface with slip properties. The effects of thermal radiation on mixed convection flow and heat transfer are significant in several processes occurring at high temperature in engineering areas and so knowledge of radiation heat transfer becomes very significant exclusively for building reliable devices in various fields like in nuclear plants, gas turbines, satellites, various propulsion devices for aircraft,

missiles and space vehicles (Ibrahim and Suneetha, 2014; Parida *et al*., 2015 [22]; Mabood and Das, 2016 [20]; Fatunmbi and Adeniyan, 2020).

The current investigation aims to examine the consequence of flow and heat transfer mechanism in a quadratic mixed convection magneto-micropolar nanofluid induced by an expanded stretching in the presence of thermo-migration and brownian motion of tiny particles, thermal radiation, viscous dissipation and Ohmic heating effect. This study finds useful applications in various industries and engineering processes such as in pharmaceutical and transportation industries, extrusion of polymers, wire drawing, paper and textile manufacturing and other metallurgical activities. The main equations are solved numerically and various parameters effects are displayed using various graphs with appropriate discussions of results.

2. Problem Formulation
For the development of the problem at hand, the following assumptions hold valid:
The flow is incompressible and steady while the working fluid is electro-conducting micropolar fluid with tiny nanoparticles. The flow is induced by vertical stretching of the sheet in x direction while y axis is perpendicular to it as pictured in the flow configuration (Fig 1).
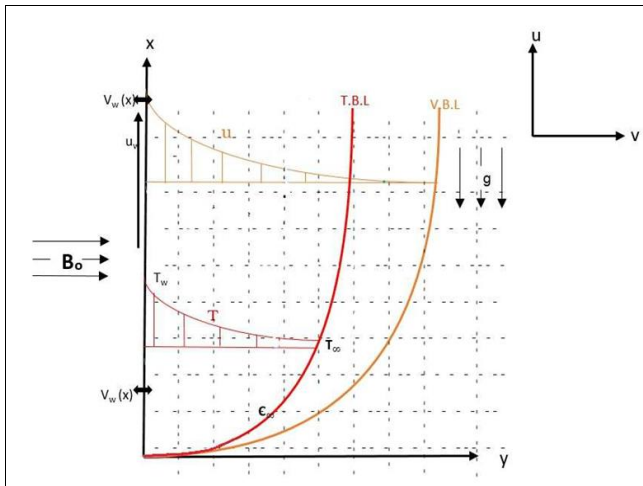

Fig 1: Schematic flow configuration

The sheet velocity is assumed to be $u = u_w$ where $u_w = cx$ and c is a positive constant indicating the rate of stretching. The heat profile is conditioned by joule heating, viscous dissipation, thermophoresis effect, Brownian motion, and thermal radiation. The wall thermal condition is assumed to be a Prescribed Surface Temperature (PST) expressed by $T = T_s$ where $T_s = (T_\infty + Ax^n)$ with n, T_s, T_∞ being a power law index, sheet temperature and free stream temperature respectively. The concentration field incorporates the influence of homogeneous chemical reaction of order one with brownian motion and thermophoresis factors. The micropolar fluid stress tensor and couple stress tensor are described by (see Eringen, 1966 [7]; Lukaszewicz, 1999 [16]; Chen *et al*., 2011):

$$\Gamma_{ij} = (-P + \beta_1 v_{k,k})\delta_{ij} + \mu(v_{i,j} + v_{j,i}) + \xi(v_{j,i} - v_{i,j}) - \beta\epsilon_{kij}\zeta_k. \tag{1}$$

$$B_{ij} = c_o\zeta_{k,k}\delta_{ij} + c_d(\zeta_{i,j} + \zeta_{j,i}) + c_a(\zeta_{i,j} - \zeta_{j,i}). \tag{2}$$

Where the symmetric part of the stress tensor is indicated by $\Gamma_{ij}^s = (-P + \beta_1 v_{k,k})\delta_{ij} + \mu(v_{i,j} + v_{j,i})$. Moreover, Γ_{ij} indicates the Cauchy stress tensor, P connotes pressure, β_1 is the second viscosity coefficient, μ stands for the dynamic viscosity, ξ expresses the dynamic microrotation viscosity, c_0, c_a and c_d are the coefficients of angular viscosity, v_i, ζ_r and ϵ_{ijk} are the velocity component, angular velocity component and the alternating/permutation stress tensor, B_{ij} is the couple stress tensor, δ_{ij} indicates Kronecker delta, $v_{i,j} = \frac{\partial v_i}{\partial x_j}, \zeta_{i,j} = \frac{\partial \zeta_i}{\partial x_j}$ describe partial derivatives with respect to coordinates (x_1, x_2, x_3). The following inequalities must hold for Eq. (1) to be satisfied: $\mu \geq 0, 3\lambda + 2\mu \geq 0, \beta \geq 0$.

2.1 The Governing Equations
The equations modelling the flow and heat transfer analysis are the continuity equation, momentum equation, microrotation equation, energy equation and concentration equation. Use has been made of the boundary layer approximations and the aforementioned assumptions for the derivation of the governing equations.

$$\frac{\partial u}{\partial x} = -\frac{\partial v}{\partial y}, \tag{3}$$

$$\rho_f\left(u\frac{\partial u}{\partial x} + v\frac{\partial u}{\partial y}\right) = g[\alpha_1(T - T_\infty) + \alpha_2(T - T_\infty)^2] + g[\beta_1(C - C_\infty) + \beta_2(C - C_\infty)^2]$$
$$+ (\mu_f + k_r)\frac{\partial^2 u}{\partial y^2} + k_r\frac{\partial \zeta}{\partial y} - \sigma B_o^2 u, \tag{4}$$

$$u\frac{\partial \zeta}{\partial x} + v\frac{\partial \zeta}{\partial y} - \frac{\gamma}{\rho_f j}\frac{\partial^2 \zeta}{\partial y^2} = -\frac{kr}{\rho_f j}\left(2\zeta + \frac{\partial u}{\partial y}\right), \tag{5}$$

$$u\frac{\partial T}{\partial x} + v\frac{\partial T}{\partial y} - \frac{k_f}{(\rho c_p)_f}\frac{\partial^2 T}{\partial y^2} = X\left(\frac{\partial T}{\partial y}\right)\left[\frac{D_T}{T_\infty}\left(\frac{\partial T}{\partial y}\right) + D_B\left(\frac{\partial T}{\partial y}\frac{\partial c}{\partial y}\right)\right].$$
$$+ \frac{(\mu_f + kr)}{(\rho c_p)_f}\left(\frac{\partial u}{\partial y}\right)^2 + \frac{\sigma B_0^2}{(\rho c_p)_f}u^2 + \frac{16\sigma^*T_\infty}{3h(\rho c_p)_f}\frac{\partial^2 T}{\partial y^2}, \tag{6}$$

$$u\frac{\partial C}{\partial x} + v\frac{\partial C}{\partial y} = D_B\frac{\partial^2 C}{\partial y^2} + \frac{D_T}{T_\infty}\left(\frac{\partial^2 T}{\partial y^2}\right) - C_r(C - C_\infty). \tag{7}$$

Subject to the following wall conditions.

$$u(x,0) = u_w, v(x,0) = 0, \zeta(x,0) = -b\frac{\partial u}{\partial y}, T(x,0) = T_s, C(x,0) = C_s,$$
$$u(x,\infty), \zeta(x,\infty), T(x,T_\infty), C(x,C_\infty) \tag{8}$$

Where x and y are the coordinates and $u, v, T, v_f, \rho_f, C, g, h$ and k_f are velocity component in x direction, velocity component in y, temperature, kinematic viscosity, density, concentration of nanoparticles, acceleration due to gravity, mean absorption coefficient and thermal conductivity respectively. The others symbols are σ which is electrical conductivity, j is the micro inertia density, $(\rho c_p)_f$ denotes the heat capacity of the fluid, ξ is the spin gradient viscosity, α_1 is the coefficient of linear thermal expansion, α_2 coefficient of nonlinear thermal expansion, β_1 is the coefficient of linear solutal expansion and β_2 is the coefficient of nonlinear solutal expansion, k_f indicates thermal conductivity, C_∞ concentration at the free stream, k_r vortex viscosity, D_B Brownian diffusion coefficient, D_T stands for thermophoretic diffusion coefficient, $\Gamma = \frac{(\rho c_p)_p}{(\rho c_p)_f}, \mu_f$

illustrates the dynamic viscosity, ζ microrotation component. Besides, the micropolar surface parameter is indicated by b in equation (6). The interval of b is given as $0 \le b \le 1$. There are various information from the value of b. For instance, when $b = 0$, then $\zeta = 0$ which implies a strong concentration of the micro-elements at the wall whereas $b = 1/2$ indicates a weak concentration of the micro-elements. In the case of $b = 1$ as it is applicable to turbulence flow situations (Peddieson, 1972, Jena and Mathur, 1981; Ahmadi, 1976).

2.2 Similarity variables
The following similarity quantities are imposed on the governing equations to transform them from partial into ordinary differential equations.

$$\eta = y\sqrt{\frac{c}{v_f}}, \psi = f(\eta)\sqrt{cv_f}\,x, \zeta = cg(\eta)\sqrt{\frac{c}{v_f}}\,x, \xi = \left(\mu_f + \frac{kr}{2}\right)j,$$
$$\theta(\eta) = \frac{T - T_\infty}{T_s - T_\infty}, \phi(\eta) = \frac{C - C_\infty}{C_s - C_\infty}, jc = v_f. \tag{9}$$

On the use of (9) the continuity equation is satisfied and equations (2-5) can be written as

$$(1+R)\frac{d^3 f}{d\eta^3} + \frac{df}{d\eta}\frac{d^2 f}{d\eta^2} - \left(\frac{df}{d\eta}\right)^2 + R\frac{dg}{d\eta} - H\frac{df}{d\eta} + \lambda_1\theta(1+\delta_1\theta) + \lambda_2\phi\beta(1+\delta_2\phi) = 0, \tag{10}$$

$$(1 + R/2)\frac{d^2 g}{d\eta^2} + f\frac{dg}{d\eta} - g\frac{df}{d\eta} - R\left(2g + \frac{d^2 f}{d\eta^2}\right) = 0, \tag{11}$$

$$(1 + Ra)\frac{d^2\theta}{d\eta} + PrEcH \tag{12}$$

$$\frac{d^2\phi}{d\eta^2} + Scf\frac{d\phi}{d\eta} - ScK\phi + \frac{Nt}{Nb}\frac{d^2\theta}{d\eta^2} = 0. \tag{13}$$

subject to:

$$\text{at } \eta = 0: \frac{df}{d\eta} = 1, f(\eta) = 0, g(\eta) = -b\frac{d^2 f}{d\eta^2}, \theta(\eta) = 1, \phi(\eta) = 1$$
$$\text{as } \eta \to \infty: \frac{df}{d\eta} = 0 \; g(\eta) = 0, \theta(\eta) = 0, \phi(\eta) = 0. \tag{14}$$

Where

$$R = \frac{kr}{\mu_f}, Pr = \frac{\mu_f c_p}{k_f}, H = \frac{\sigma B_0^2}{c\rho_f}, Ra = \frac{16\sigma^* T_\infty^3}{3k^* k_\infty}, Ec = \frac{u_w^2}{c_p(T_s - T_\infty)}, \lambda_1 = \frac{Gr_x^2}{Re_x}, \beta = \frac{Gc_x}{Gr_x},$$
$$\lambda_2 = \frac{Gc_x^2}{Re_x}, Sc = \frac{v_f}{D_B}, K = \frac{C_r}{c}, Nt = \frac{D_T\Gamma(T_s - T_\infty)}{T_\infty v_f}, Nb = \frac{D_B\Gamma(C_s - C_\infty)}{v_f}, \delta_1 = \frac{\alpha_2(T_s - T_\infty)}{\lambda_1},$$
$$\delta_2 = \frac{\beta_2(C_s - C_\infty)}{\lambda_1}, Gr_x = \frac{g\alpha_1(T_s - T_\infty)}{c^2 x}, Gc_x = \frac{g\beta_1(C_s - C_\infty)}{c^2 x}. \tag{15}$$

In equation (13), R is the material micropolar term, Pr represents Prandtl number, H is the magnetic field term, Ra is the radiation parameter, Ec shows Eckert number, Sc denotes the Schmidt number, $G_c x$ local solutal Grashof number, $G_r x$ local thermal Grashof number, δ_1 nonlinear thermal convection, δ_2 nonlinear concentration convection, K chemical reaction term, λ_1 mixed convection parameter, λ_2 mass mixed convection parameter, β indicates ratio of concentration to buoyancy forces, Nt is the thermophoresis term and Nb indicates the Brownian motion sequentially.

2.3 Quantities of engineering interest
For the quantities of engineering interest in this study, the coefficient of skin friction S_{fx} which corresponds to the viscous drag at the wall, the Nusselt number Hu_x which implies the heat transfer at the surface and the Sherwood

number Sh_x. These quantities are respectively communicated in Eq. (14) as

$$S_{fx} = \frac{\tau_w}{\rho_f u_w^2}, Hu_x = \frac{xQ_w}{\kappa(T_s - T_\infty)}, Sh_x = \frac{xQ_m}{D_B(C_s - C_\infty)}. \tag{14}$$

Using the similarity variables (7) on equation (14) to obtain the dimensionless version of the quantities of engineering interest which are written as

$$C_{fx} = [1 + (1-b)R]Re_x^{-1/2}\frac{d^2 f}{d\eta^2} \text{ at } \eta = 0, \tag{15}$$

$$Nu_x = -(1 + Ra)Re_x^{1/2}\frac{d\theta}{d\eta} \text{ at } \eta = 0, \tag{16}$$

$$Sh_x = -Re_x^{1/2}\frac{d\phi}{d\eta} \text{ at } \eta = 0. \tag{17}$$

Where $\tau_w = \left(\left(\mu_f + kr\right)\frac{\partial u}{\partial y} + \mu_f\zeta\right)_{y=0}$, $Q_w = -\left[\left(k_f + \frac{16T_\infty^3\sigma^*}{3h}\right)\frac{\partial T}{\partial y}\right]_{y=0}$

and $Q_m = -D_B\left(\frac{\partial c}{\partial y}\right)_{y=0}$ indicates shear stress, heat flux and mass flux in that order.

3. Method of solution
In view of the high nonlinearity of the governing equations (10-13) subject to the wall conditions (14), a numerical solution to the controlling equations is sought by means of Runge-Kutta-Fehlberg in conjunction with shooting techniques. This method has been suitable for nonlinear ordinary differential equations due to its accuracy and stability. The details of this method can be found in the reports of Ali (1994) [3]; Attili and Syam (2008) [4]; Mahanthesh et al., (2018) [19]. The correctness of the results obtained has been verified by comparing the values of the Nusselt number with exiting studies in literature when Prandtl number Pr and temperature exponent n vary under some limiting constraints. As collated in Table 1, there is a good agreement with the present results as compared with the existing work. The values of the dimensionless parameters have been carefully selected as follows $R = M = 0.7, Nt = Nb = 0.5, Rd = 0.3, \delta_1 = \delta_2 = 0.3, Ra = 0.3, K = 0.2, \lambda_1 = \lambda_2 = 0.6, Sc = 0.44, b = n = 0.5$ and $Pr = 0.72$. These values are used for the computation unless otherwise stated in the figures.

Table 1: Computational values of Nusselt number Hu_x for different values of Pr and n as compared with existing study

n	Grubka and Bobba (1985)		current work	
	Pr =0.72	Pr = 1.0	Pr =0.72	Pr = 1.0
- 2.0	0.7200	1.0000	0.72069	0.99945
- 1.0	0.0000	0.0000	-0.00110	0.00012
0.0	-0.4631	-0.5820	-0.46359	-0.58201
1.0	-0.8086	-1.0000	-0.80883	-1.00001
2.0	-1.0885	-1.3333	-1.08862	-1.33333
3.0	-1.3270	-1.6154	-1.32707	-1.61538

4. Results and discussion
The contributions of the various physical parameters on the dimensionless velocity profile, microrotation field, heat distribution and concentration profiles are illustrated with different graphs and appropriate discussion for better prediction and application. Fig 2-5 reveal the impact of the material parameter R on the dimensionless quantities. A rise in R causes the microrotation profile to appreciate both

in the presence or absence of the magnetic field term as found in fig 2. The microrotation profile attains the minimum level in the absence of the magnetic field $M = 0$ Thus the impact of M is to boost the microrotation field as the micropolar parameter rises in value. Likewise, growing values of R causes the velocity field to accelerate and increase the thickness of the hydrodynamic boundary layer as depicted in fig 3. With arise in R there is a decline in the strength of the dynamic viscosity and in this view, there a decline in the resistance to the fluid flow. However, the fluid motion decelerates with a rise in the strength of the magnetic field term M as shown in fig 3. This action resulted from the Lorentz force which is a drag-like force caused by the interaction between the electrically conducting micropolar fluid and the magnetic field. Thus, magnetic field impact helps in controlling the fluid motion which is applicable in engineering processes like extrusion works.

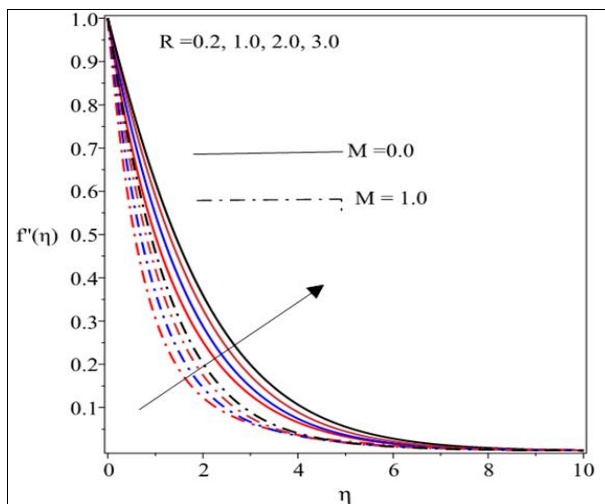**Fig: 2** Microrotation profiles for varying R

Fig 3: Velocity field for changes in R

Meanwhile, there is a fall in the thermal boundary layer thickness as well as surface heat distribution as R increase in strength in the presence or absence of the magnetic field term as depicted in fig 4. It is also shown that the thermal region is escalated due to higher M because of the additional heat created due to friction occasioned by the flow

resistance induced by the Lorentz force. In the same manner, the concentration layer decline with higher magnitude of R as displayed in fig 5.
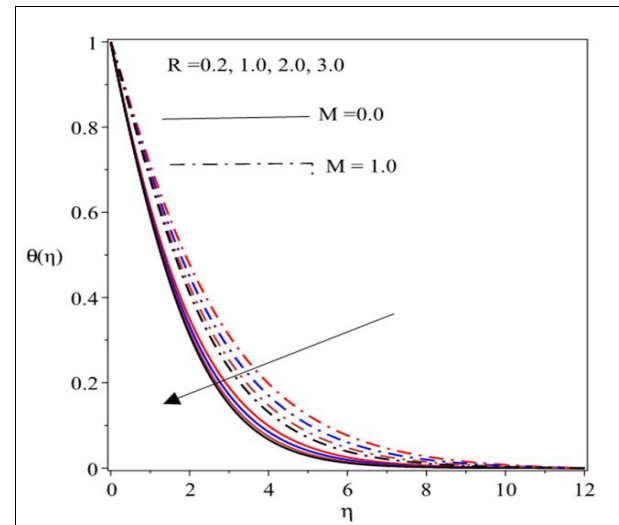

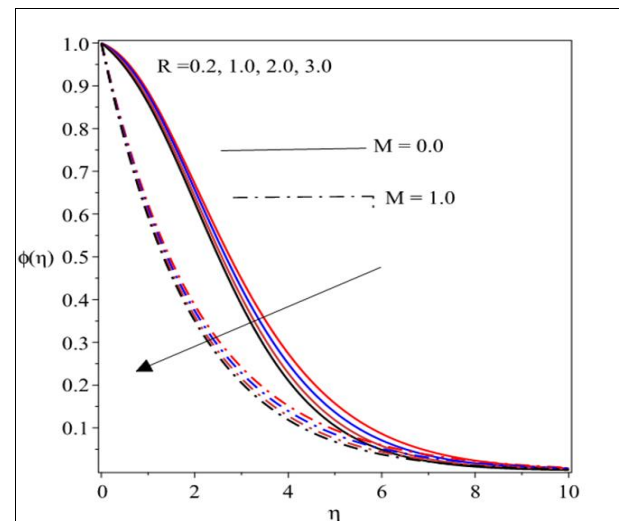**Fig 4:** Plot of thermal field against R

Fig 5: Concentration profile for variation in R

In the absence of M there is a thicker concentration boundary layer and a higher profile as compared to the presence of M. Fig 6 and 7 respectively demonstrate the impact of the mixed convection parameter λ on the velocity and temperature profiles in the presence of the nonlinear thermal convection δ_1 A rise in λ energizes the buoyancy force and dominates the viscous force and consequently propels arise in the fluid motion. This response is due to the fact that arise in λ favours the buoyancy force and causes a reduction in the viscous force as shown in fig 6. However, the converse is the case on the temperature distribution across the boundary layer as illustrated in fig 7.

The characteristics of concentration mixed parameter λ_2 on the transport fields of velocity and concentration are demonstrated in fig 8 and 9 respectively in the presence of nonlinear concentration convection term δ_2 Similar to the reactions discussed in fig 6 and 7, a rise in λ_2 enhances the velocity profile. This trend occurs due to the dominance of the buoyancy force on the viscous force as λ_2 increases. The concentration field on the other hand depreciates with
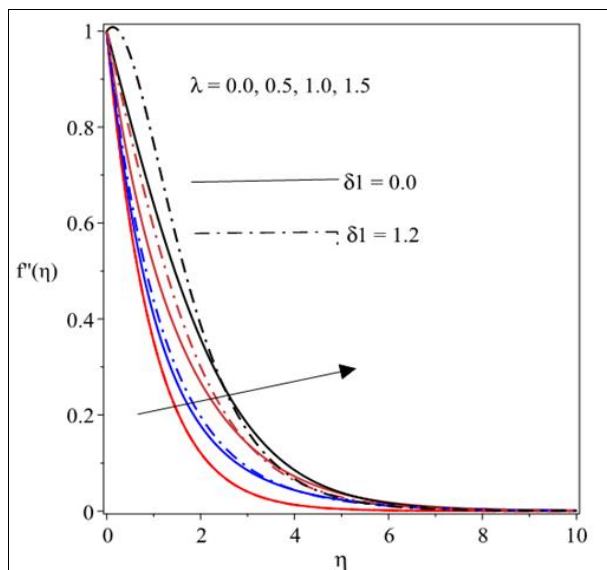
enhancement of λ_2 as clearly shown in fig 9.

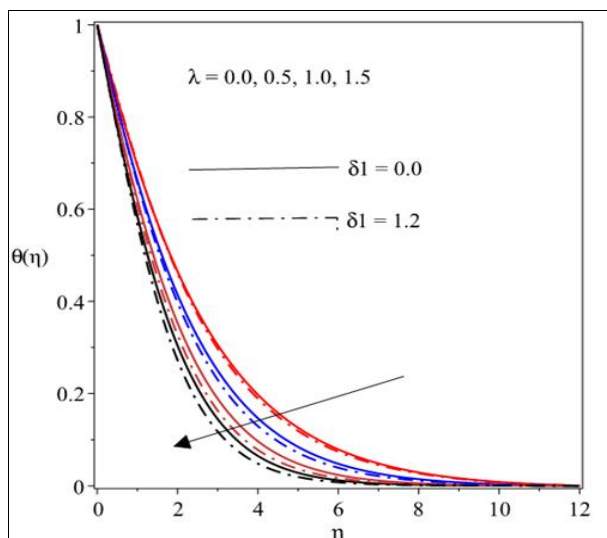**Fig 6:** Velocity field for variation in λ

Fig 7: Temperature distribution for changes in λ

Fig 10 and 11 are plotted to reveal the impact of the Prandtl number Pr on the velocity and temperature profiles in the presence and absence of the Eckert number Ec As found in fig 10, there is a decline in the fluid motion as Pr increases when Ec and when $Ec = 1.0$ This trend occurs due to the fact that growth in Pr corresponds to a rise in the dynamic viscosity of the fluid and in this view, there is a resistance to the fluid motion and a decelerated flow. Likewise, the thermal boundary layer shrinks as Pr rises in magnitude and in consequence, the surface temperature drops as depicted in fig 11. Here, there is a decline in the thermal diffusivity and a rise in the momentum diffusivity as Pr enhances and such trend leads to a reduction in the temperature distribution. On the other hand, as Ec increases, the thermal field appreciates due to friction between the micropolar fluid particles and the stretching sheet which creates additional heat in the flow region.
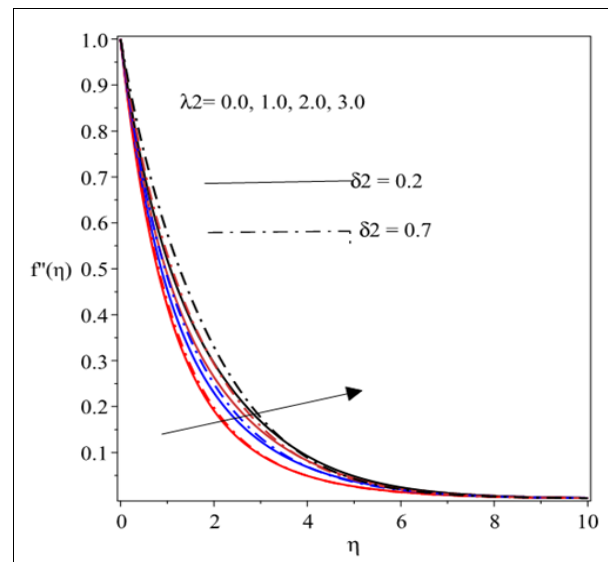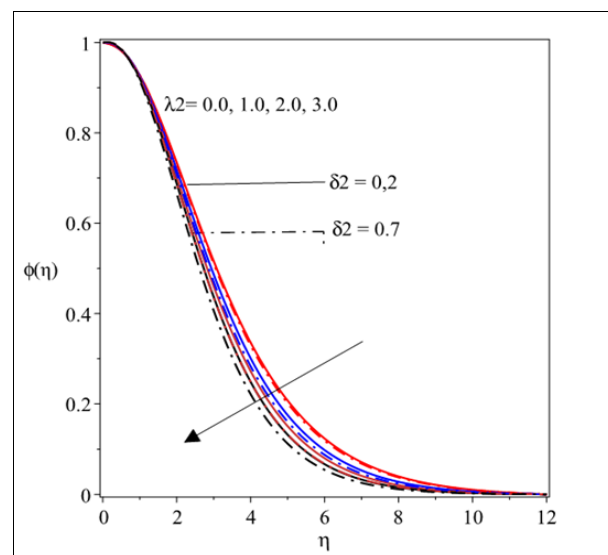

Fig 8: Plot of velocity profiles against λ_2

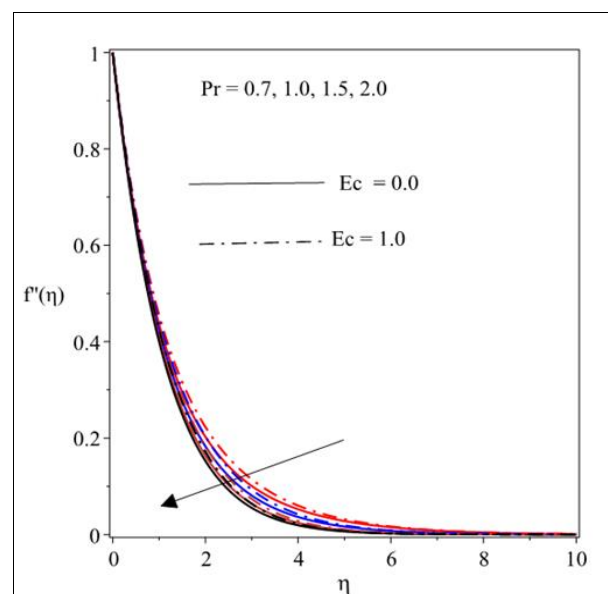**Fig 9:** Concentration profiles for λ_2
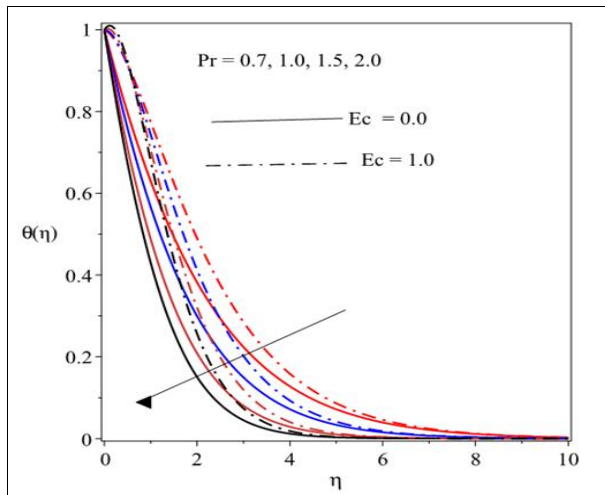

Fig 10: Velocity field versus Pr

Fig 11: Temperature profiles versus Pr

The graph of temperature distribution versus η for variation in the radiation parameter Ra is shown in fig 12 in the presence and absence of the temperature exponent term n the heat region as demonstrated in fig 12. It is clearly seen that the heat distribution appreciates as Ra escalates in magnitude. There is a positive impact on the heat conduction due to a growth in Ra and as such, a boost the heat profile. A rise in the thermophoresis parameter Nt raises the concentration profile and thickens the solutal boundary layer as demonstrated in fig 13. However, the concentration field $\phi(\eta)$ decreases as the Schmidt number Sc rises in magnitude. Thermophoresis force promotes a rise in the temperature profile due to the temperature gradient occasioned by the thermophoretic force, such a force propels higher flow further away from the sheet such that more heated fluid is drawn away from the sheet which consequently causes a rise in thermal field as Nt advances. The reaction of the Brownian motion term Nb in respect to temperature distribution is displayed in fig 14. Brownian movement is the irregular motion found in the nanoparticles by its suspension in the working fluid. Due to this irregular motion, there is an increase in the kinetic energy due to the enhanced motion of the fluid and as such, there is arise in the temperature of the fluid as noticed in this figure.
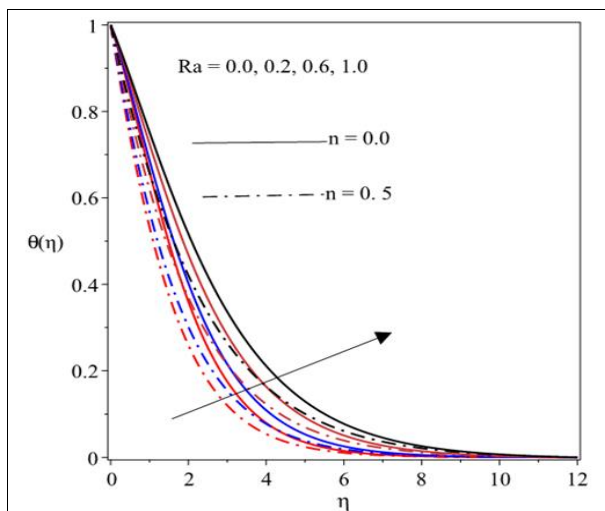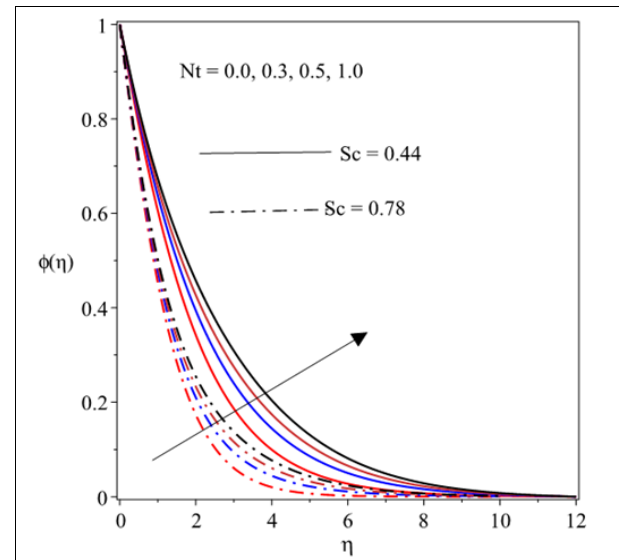

Fig 12: Temperature distribution versus Ra

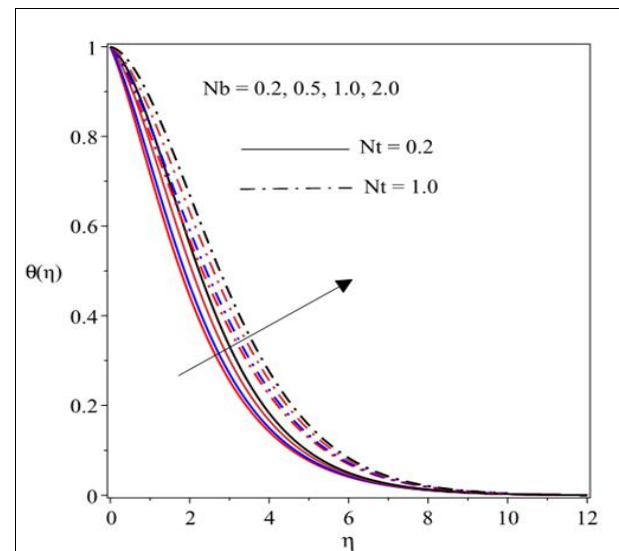**Fig 13:** Concentration profiles versus Nt

Fig 14: temperature profiles for variation in Nb

5. Conclusion

The analysis carried out in this study is based on the quadratic mixed convection flow and heat propagation of magneto-micropolar nanofluid over a vertically extending sheet. In the model considered, the impact of viscous dissipation, Ohmic heating, thermal radiation, thermophoresis and Brownian motion are incorporated in the presence of the prescribed surface temperature at the thermal boundary. The mathematical equations have been reduced from partial into ordinary derivatives by means of the relevant similarity quantities while the reduced system of equations has been solved numerically via the scheme of the Runge-Kutta Fehlberg and shooting technique. The reliability of the codes is verified by comparing the computational values of the Nusselt number obtained in this study with existing related study in the literature under some limiting scenarios. Summarily, the study reveals that:

- The microrotation boundary layer thickness and the hydrodynamic boundary layer expands as the micropolar material parameter R increases which in turn leads to fluid motion acceleration in the transport field.
- The thermal and concentration profiles drastically reduced as micropolar term enhances whereas the

opposite is the case as the magnetic field parameter increases in magnitude. The magnetic field term boost temperature distribution but decelerate velocity profiles.

- Both the thermal and momentum boundary layer thickness depreciate as the Prandtl number Pr increases and so, the there is a reduction in the micropolar nanofluid motion and the surface temperature also falls with higher Prandtl number.
- The temperature and nanoparticle concentration boundary layer appreciate with growth in the thermophoresis and brownian motion terms but the reverse is the case for growth in the Schmidt number and brownian motion terms on the concentration profiles.
- An expanded thermal boundary layer is encountered as the radiation and Eckert number terms increase in magnitude but the thermal field decrease with growth in the temperature exponent parameter.

6. References

1. Akbar NS, Nadeem S, Haq RU, Khan M. Radiation effects on MHD stagnation point flow of nanofluid towards a stretching surface with convective boundary condition, Chinese Journal of Aeronautics. 2013; 26(6):1389-1397.
2. Akinbobola TE, Okoya SS. The flow of second grade fluid over a stretching sheet with variable thermal conductivity and viscosity in the presence of heat source/sink, Journal of the Nigerian Mathematical Society. 2015; 34:331-342.
3. Ali ME. Heat transfer characteristics of a continuous stretching surface, Warme-und Stoffubertragung. 1994; 29(4);227-234.
4. Attili BS, Syam ML. Efficient shooting method for solving two-point boundary value problems, Chaos, Solitons and Fractals. 2008; 35(5):895-903.
5. Crane LJ. Flow past a stretching plate. Communicatios Breves. 1970; 21:645-647.
6. Eringen AC. Simple microfluids. International Journal of Engineering Science. 1964; 2(2):205-217.
7. Eringen AC. Theory of micropolar fluids. J. Math. Anal. Appl. 1966; 16:1-18.
8. Eringen AC. Theory of thermo-microfluids. Journal of Mathematical Analysis and Applications. 1972; 38:480-496.
9. Das K, Jana S, Kundu PK. Thermophoretic MHD slip flow over a permeable surface with variable fluid properties, Alexandria Engineering Journal. 2015; 54:35-44.
10. Fatunmbi EO, Fenuga OJ. MHD micropolar fluid flow over a permeable stretching sheet in the presence of variable viscosity and thermal conductivity with Soret and Dufour effects. International Journal of Mathematical Analysis and Optimization: Theory and Applications, 2017, 211-232.
11. Fatunmbi EO, Adeniyan A. MHD stagnation point-flow of micropolar fluid past a permeable stretching plate in porous media with thermal radiation, chemical reaction and viscous dissipation. Journal of Advances in Mathematics and Comp Science. 2018; 26(1):1-19.
12. Gupta PS, Gupta AS. Heat and mass transfer on a stretching sheet with suction or blowing. Can. J. Chem. Eng. 1977; 55:744-746.
13. Khan MI, Hayat T, Khan MI, Alsaedi A. Activation energy impact in nonlinear radiative stagnation point flow of cross nanofluid, International Communications in Heat and Mass Transfer. 2018; 91:216-224.
14. Kumar L. Finite element analysis of combined heat and mass transfer in hydromagnetic micropolar flow along a stretching sheet. Comput Mater Sci. 2009; 46:841-848. Doi: 10.1371/journal.pone.0059393
15. Kumar RVMSSK, Kumar GV, Raju CSK, Shehzad SA, Varma SVKJ. Analysis of Arrhenius activation energy in magnetohydrodynamic Carreau fluid flow through improved theory of heat diffusion and binary chemical reaction, Phys. Commun. 2018; 2:1-15.
16. Lukaszewicz G. Micropolar fluids: Theory and Applications (1st Ed.). Birkhauser, Boston, 1999.
17. Mabood F, Ibrahim SM, Khan WA. Effect of melting and heat generation/absorption on Sisko nanofluid over a stretching surface with nonlinear radiation. Physica Scripta. 2019; 94(6):065701.
18. Makinde OD, Aziz A. Boundary layer flow of a nanofluid past a stretching sheet with a convective boundary condition. International Journal of Thermal Sciences. 2011; 50:1326-1332.
19. Mahanthesh B, Gireesha BJ, Gorla RSR, Makinde OD. Magnetohydrodynamic three-dimensional flow of nanofluids with slip and thermal radiation over a nonlinear stretching sheet: A numerical study, Neural Computing and Applications. 2018; 30(5):1557-1567.
20. Mabood F, Das K. Melting heat transfer on hydromagnetic flow of a nanofluid over a stretching sheet with radiation and second order slip, Eur. Phys. J. Plus. 2016; 131(3).
21. Noor NFM, Haq RU, Nadeem S, Hashim I. Mixed convection stagnation flow of a micropolar nanofluid along a vertically stretching surface with slip effects, Meccanica, 2015, 1-16.
22. Parida SK, Panda Rout S, BR. MHD boundary layer slip flow and radiative nonlinear heat transfer over a flat plate with variable fluid properties and thermophoresis, Alexandria Engineering Journal. 2015; 54:941-953.
23. Qasim M, Khan I, Shafle S. Heat transfer in a micropolar fluid over a stretching sheet with Newtonian heating. Plos One. 2013; 8(4):1-6.
24. Ramzan M, Ullah N, Chung JD, Lu D, Farooq U. Buoyancy effects on the radiative magneto micropolar nanofluid flow with double stratification, activation energy and binary chemical reaction, Scientific Reports. 2018; 7:1-15.
25. Reena, Rana US. Effect of Dust Particles on rotating micropolar fluid heated from below saturating a porous medium. Applications and Applied Mathematics: An International Journal. 2009; 4:189-217.
26. Vajravelu K. Viscous flow over a nonlinearly stretching sheet., Appl. Math. Comput. 2001; 124:281-288.
27. Xu L, Lee EWM. Variational iteration method for the magnetohydrodynamic flow over a nonlinear stretching sheet. Abst Appl Anal 5 pages, 2013.